THE JOURNAL OF PHYSICAL CHEMISTRY C

Article

pubs.acs.org/JPCC

Nanopatterned Substrates Increase Surface Sensitivity for Real-Time Biosensing

Julia Y. Lin,[†] Andreea D. Stuparu,[†] Mark D. Huntington,[‡] Milan Mrksich,[†,§,⊥] and Teri W. Odom*[,†,‡]

Departments of [†]Chemistry, [‡]Materials Science and Engineering, [§]Biomedical Engineering, and [⊥]Cell and Molecular Biology, Northwestern University, Evanston, Illinois 60208, United States

ABSTRACT: In this paper, we report critical design rules for improving the sensitivity of plasmonic biosensors. We use a scalable, parallel method to fabricate Au plasmonic crystal substrates patterned with an array of pits for real-time sensing. Capture ligands printed selectively in these pits resulted in a strong response to the binding of macromolecules. Angle-resolved sensorgrams showed quantitative differences between wavelength shifts produced by protein analyte bound within regions supporting localized and long-range electromagnetic fields. Contributions from the localized fields dominated the sensing response, especially at high angles. The angle-dependent far-field and near-field optical properties of selectively functionalized plasmonic crystals suggest that optimal performance is achieved at excitation parameters that produce an intense resonance with narrow spectral bandwidth and highly localized electromagnetic fields.

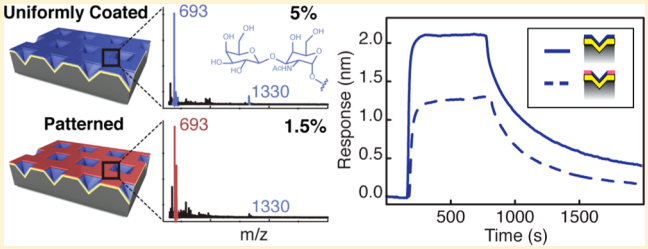

Plasmonic substrates are promising platforms for investigating design parameters that could improve the sensitivity of label-free biosensors. Maximizing the overlap of the surface plasmon fields with the molecular analyte is crucial for the detection of low concentration targets.[1] Discrete metallic nanostructures have pushed the limits of plasmonic biosensing because they support nonpropagating, localized surface plasmons (LSPs) characterized by short (10−80 nm) electromagnetic (EM) decay lengths that are on the scale of biomolecules.[2] Specifically, noble metal nanoparticles with anisotropic shapes[3−8] have demonstrated individual antibody[4,5] and protein[7,8] detection at the single particle level.

Fundamentally, the sensing contributions from single particle LSPs are not well characterized because the molecules can bind anywhere on the particle surface, both inside and outside the localized fields. Masking techniques can facilitate the binding of analyte to ligands placed in the hot spots on fabricated structures, such as nanoholes[9−12] and random nanodisk arrays,[13] to test the sensing response from only the localized fields. These local fields can, in principle, show higher performance on a per molecule basis. For example, a dielectric layer can be deposited on top of Au nanohole arrays to block adsorption to the flat film and confine binding exclusively to within the holes.[9,11] Despite a greater than 4-fold increase in sensitivity from selective surface functionalization,[13] arrays of nanoparticles and nanoholes are less sensitive than surface plasmon resonance (SPR) spectroscopy because of low signal and resolution.

Engineered metal films that support propagating EM fields called surface plasmon polaritons (SPPs) exhibit high signal-to-noise ratios with a resolution more practical in the broader scope of device integration. Plasmonic crystals, a new class of SPP-based sensors, are grating substrates that can consist of 2D arrays of three-dimensional (3D) features, including pits of various shapes.[14,15] The surface topography offers distinct advantages for sensing by allowing both SPPs and localized electric fields[14−17] to be supported simultaneously. Hence, plasmonic crystals are an ideal substrate to determine how much the localized EM fields and SPPs each contribute in biosensing. The challenge of immobilizing capture ligands in distinct sensing regions on continuous surfaces, however, has made the execution of these studies difficult.

Here we show how patterning the capture ligand only in the high electric field regions can enhance the surface sensitivity of plasmonic crystal substrates with 3D pits. By monitoring the real-time binding of a lectin analyte with a surface that presents disaccharide capture ligands, we demonstrated that local field enhancements enabled the detection of fewer than ten biomolecules per pit. This lectin−disaccharide model system has been previously optimized for biosensing,[18,19] and has a micromolar affinity[20] that enables kinetic analysis for comparison with SPR. We determined that selective patterning was critical for improving the performance of SPP-based sensors. In addition, we found that (i) optimal sensor performance could be achieved by carefully choosing an excitation angle that generated both highly confined localized EM fields and high sensitivity, and (ii) the lower limit of detection for the plasmonic crystals was reached by analytes greater than 36 kDa.

Received: February 14, 2013
Revised: February 20, 2013
Published: February 21, 2013

   dx.doi.org/10.1021/jp401598a | J. Phys. Chem. C 2013, 117, 5286−5292

EXPERIMENTAL AND THEORETICAL METHODS

Fabrication of Au Plasmonic Crystals. Two types of Au plasmonic crystals were created by using a process known as PEEL (phase shifting photolithography, etching, e-beam, and lift-off).[21,22] First, we patterned a hexagonal array of circular photoresist posts (d = 150 nm, a_0 = 400 nm) on a Si (100) wafer. A layer of Cr (10 nm) was then deposited on the surface by e-beam, and the photoresist was lifted off to result in a Cr hole array through which the underlying Si was anisotropically etched to form a template of pyramidal pits on which Au (50 nm) was deposited line-of-sight. To create the triangular prism plasmonic crystals, Si wafers with (111) crystallinity were patterned. The Si was etched isotropically through the metal hole array film by deep reactive ion etching (DRIE) for 15−20 s to achieve ∼50 nm deep wells. The substrates were subsequently exposed for 10−15 s to an aqueous 6 M potassium hydroxide (Sigma-Aldrich, Inc.) solution heated to 80 °C to render vertical sidewalls and a flat base for the triangular prism geometry. Finally, the Cr layer was removed from the Si, and Au was deposited on the Si to form the plasmonic crystals. To cover the Si template with a conformal film of Au, we mounted the Si chip onto a home-built, angled, rotating stage (at 37.6°) compatible with our thermal evaporator.

Preparation of Plasmonic Crystals for Sensing. Uniformly coated surfaces were prepared by immersing the plasmonic crystal in a 5% ethanolic solution of maleimide and 95% tri(ethylene glycol) (EG3)-terminated mixed disulfides (0.2 mM final disulfide concentration) overnight at 4 °C. The patterned substrates were functionalized by first patterning the EG3-terminated disulfides via contact printing for 15−20 s with a flat PDMS slab, followed by immersion in an ethanolic solution of 5% (by concentration) maleimide solution as described above for the uniformly coated substrates. Following the self-assembly of the maleimide-EG3 monolayers, the substrates were reacted with a 0.1 mM thiol-terminated disaccharide solution (Tris buffer, pH 7.5) for 1 h at room temperature. We used the Galβ(1, 3)GalNAc disaccharide for the peanut agglutinin binding experiments and GlcNAcβ(1, 4)GlcNAc for wheat germ agglutinin. The substrates for the control SPR experiments using Biacore 2000 (GE Healthcare) were prepared similarly, but instead of plasmonic crystals, we used gold (100 nm Au) deposited on Ti-coated (10 nm) glass slides.

Characterization of Functionalized Plasmonic Crystal Surfaces. Self-assembled monolayer matrix-assisted laser desorption ionization mass spectrometry (SAMDI MS) was used to characterize and quantify the surface density of the molecular monolayers assembled on the plasmonic crystals for biosensing. The maleimide- and EG3-terminated disulfides for the mixed monolayers were purchased from Chemtos; the disaccharides were synthesized according to previously described methods.[23,24] The corresponding proteins—peanut and wheat germ agglutinins (Sigma-Aldrich, Inc.)—were dissolved in Dulbecco's phosphate buffer (Invitrogen; pH 7.4) to 0.625−5 μM concentrations. Measurements were performed with an Applied Biosystems 4800 MALDI TOF mass spectrometer. A 355-nm Nd:YAG laser was used as the desorption/ionization source. The spectra for the maleimide/EG3 and disaccharide monolayers were acquired by using the reflector positive mode and 2′,4′,6′-trihydroxyacetophenone monohydrate (Sigma-Aldrich, Inc.; 30 mg/mL in acetone) as matrix. The lectin spectra were collected in the high mass linear mode and sinapic acid (Sigma-Aldrich, Inc.; 10 mg/mL in acetone) was used as the matrix. Each spectrum was the average of 800 shots.

To determine surface coverage, the Data Explorer (Applied Biosystems) software was used to integrate the area under the disaccharide (m/z 1330 for Galβ(1, 3)GalNAc and m/z 1371 for GlcNAcβ(1, 4)GlcNAc) and EG3 disulfide (m/z 693) peaks. The percent coverage of the disaccharide was calculated by dividing the disaccharide peak area by the sum of the total areas of the disaccharide and EG3 disulfide peaks. The surface coverage ratio of the patterned vs nonpatterned surfaces was determined by dividing the percent disaccharide coverage determined from the spectra from patterned substrates by the percent coverage found for the nonpatterned substrates. The EG3 disulfide was used as an internal standard for the calculation because the integrated values for the peaks in the MALDI spectra are not quantitative.

Optical Properties of Plasmonic Crystals. Angle-resolved spectra were measured in a pseudobiological environment with use of a home-built rotating stage coupled via an optical fiber cable to a spectrometer attached to a thermoelectrically cooled CCD (Princeton Instruments). Broadband white light (p-polarized) from a tungsten-halogen lamp was used to illuminate the sample at incident angles θ. The reflected light was dispersed by a 300 BLZ = 500 nm grating and collected by the CCD. To characterize the optical properties of the plasmonic crystals in phosphate buffer (n = 1.334), a liquid holding cell was fabricated by sandwiching a silicone sheet (Grace Bio Laboratories, thickness = 250 μm) with a square (4 mm × 4 mm) window; a drop of buffer was suspended between the substrate and the glass microscope slide. Reflectance spectra of the plasmonic crystals and a flat Au substrate background were collected at each angle. Because the spectra were normalized to the reflectivity from the Au reference film, any effects from the glass (top) surface are negligible.

Finite Difference Time Domain (FDTD) Calculations. FDTD methods (Lumerical Inc.) were used to calculate the angle-resolved reflection spectra from θ = 10°−60° for each of the plasmonic crystals. The phosphate buffer overlayer was applied as a dielectric slab defined with a refractive index n = 1.334. A conformal mesh (grid size = 4 nm in the x-, y-, and z-directions) was set for the simulation volume that directly encloses a single pyramidal or triangular prism-shaped pit. The frequency-dependent optical constants, taken from Palik[25] (Si) and Johnson and Christy[26] (Au), were fit at the simulation wavelengths (λ = 400−1000 nm, to replicate broadband white light) with a multicoefficient model provided in the FDTD software. Bloch boundary conditions were applied in the x and y directions to simulate the 2D periodic lattice. A plane wave, linearly polarized along the direction of highest symmetry for the hexagonal array geometry, was used as the source. For the angular excitation, an angle that accounted for the bending of light as it passed through materials with different RIs was determined for corresponding experimental angles and used as the incidence angle. A 2D transmission monitor was placed above the substrate to record the light reflected from the plasmonic crystal surface.

Because nanostructure geometry can be used to tailor the near-field confinement of electromagnetic fields, we visualized the sensing hot spots in a pyramidal and triangular prism pit using FDTD computation. The electric field distribution was calculated when the plasmonic crystals were excited from θ =

dx.doi.org/10.1021/jp401598a | J. Phys. Chem. C 2013, 117, 5286−5292

10°−60° in 10° intervals. Similar source frequency, source polarization, and optical constants of the materials were used as described above. Instead of the 4-nm mesh, we used a 1-nm conformal mesh (in the x- and z-directions) in only the center plane (x−z) of the enclosed simulation volume to improve the spatial resolution of the field distribution.

Real-Time Optical Measurements of Protein Binding. Sensorgrams were generated by measuring the binding of lectin in real time. A flow channel was used to deliver the protein to the active surface of the sensor. The channel was fabricated by sandwiching a silicone sheet (Grace Bio Laboratories, thickness = 250 μm), with a 1-mm wide and 10-mm long slit cut in the center, between the plasmonic crystal and a glass microscope slide. Inlet and outlet holes were drilled through the glass slide providing openings for tubing connections (N-126S Upchurch Scientific NanoPort Assembly and 1569 PEEK Tubing). A syringe pump (kdScientific) connected to an injection valve (Rheodyne 9725) was used to introduce sample solutions with a constant flow rate of 100 (optimized for peanut agglutinin) or 200 μL/min (optimized for wheat germ agglutinin). The plasmonic crystal was first exposed to phosphate buffer for ∼150 s to establish a baseline signal. Protein was then injected at their corresponding optimal flow rates until surface saturation was reached (150−750 s). A small air bubble was artificially introduced in the flow system after the protein solution was injected to create a sharp change between the association and dissociation regions of protein binding. After 750 s, the sensor surface was washed with phosphate buffer for approximately 25−30 min to dissociate the bound lectin for kinetic analysis. Binding curves were generated from spectra collected every 0.5 s, at the slower flow rate, and 0.1 s, for faster fluid flow, using a high-resolution grating (1200 BLZ = 500 nm). The position of the resonance at each time point was determined by fitting the reflectance dip with a Lorentzian function, using MATLAB.

We compared results from our home-built sensing system with those acquired with use of the Biacore 2000 (SPR in the Kretschmann configuration) because the protein binding assay was performed under optimal flow conditions determined for each instrument. The conventional SPR experiments were run at a constant flow rate of 10 μL/min. First, phosphate buffer was exposed to the functionalized, flat Au surface for 5 min, followed by the lectin solution (5 μM for peanut agglutinin and 0.625 μM for wheat germ agglutinin) for 10 min, and then again by phosphate buffer for 15 min.

Determination of Kinetic Constants for Peanut Agglutinin. Association, dissociation, and equilibrium affinity constants were obtained from the sensorgrams. The binding curves were fit with the nonmass transport limited Langmuir model, using the Scrubber software, where 5 μM was input as the concentration of the peanut agglutinin. The association and dissociation constants were determined by fitting the binding curves from the point of protein injection (150 s) to the end of the surface association and saturation regions (∼150−750 s) and after the time point when the protein begins to dissociate from the surface (>750 s), respectively. The dissociation region in the sensorgrams was fit to the Langmuir dissociation model: $\lambda = \lambda_0 + R_0 e^{-k_d t}$, where t is time, λ is the wavelength of the resonance position, R_0 and λ_0 are constants, and k_d is the dissociation constant. The association region from protein binding was then fit to the Langmuir association model: $\lambda = [k_a C_a R_{Max}(1 - e^{(C_a R_{Max} + k_d)(t - t_0)})]/(C_a R_{Max} + k_a)$, where t_0 is the starting time, C_a is the concentration, R_{Max} is a constant, and k_a is the association constant. The affinity constant is the ratio of the association and dissociation constants.

RESULTS AND DISCUSSION

We patterned the capture ligand selectively in the pits of the Au plasmonic crystals as shown in Figure 1. To isolate the effects of the localized fields on the plasmonic crystal sensor response, we functionalized the surfaces in two ways as described in the Experimental Section. Uniformly coated surfaces were prepared by immersing the plasmonic crystal in a 5% (by concentration) ethanolic solution of a maleimide and EG3 mixed disulfide (Figure 1a, left). We used this mixed monolayer system to control the ligand density, which cannot be achieved by simply attaching the thiol-terminated disaccharides directly to Au and to form closely packed monolayers. The disulfides consisted of long alkyl chains terminated by a maleimide or an EG3 moiety. To stagger the physical placement of the end functionality, we had the maleimide presenting chain a few bonds longer than the EG3-terminated chain. Hence, the close packing of the molecules can form inert monolayers that prevent nonspecific protein adsorption.[18] Although thiol-based molecules could be used to build the monolayer, thiols exchange easily with other components in solution, and the resulting SAM would be less stable compared to those formed from disulfides. The 5% maleimide concentration was determined as the optimal ligand density to avoid any crowding or steric blocking of the disaccharides that can inhibit their binding with the active protein.[14,19]

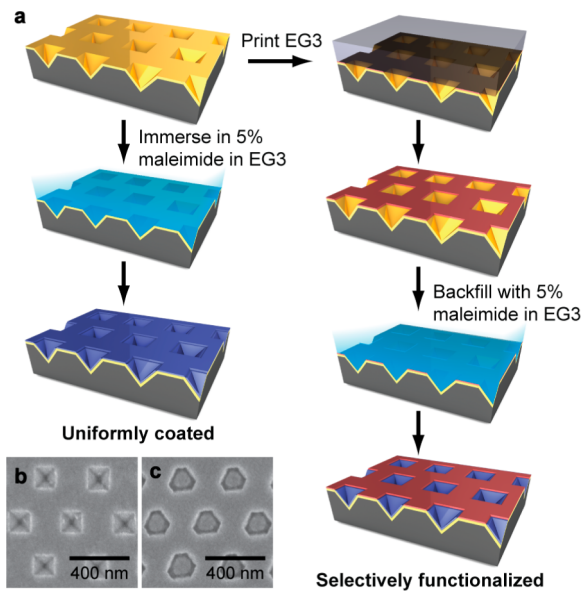

Figure 1. (a) Scheme for the preparation of uniformly coated and selectively functionalized sensing surfaces. SEM images of the substrates used for biosensing that consist of (b) pyramidal and (c) triangular unit cells in a hexagonal array (a_0 = 400 nm).

Patterning the flat Au surfaces with EG3 by contact printing directed the analyte to bind in local sensing regions. Passivating the regions around the pits with a monolayer of nonbioactive EG3 prevented nonspecific adsorption of the protein analyte to the surface and allowed us to characterize the response from the localized fields. The substrates were then treated with a 5% maleimide and EG3 solution[14] so that mixed self-assembled monolayers (SAMs) formed only in the pits (Figure 1a, right).

dx.doi.org/10.1021/jp401598a | J. Phys. Chem. C 2013, 117, 5286−5292

The monolayer-coated substrates were subsequently exposed to a thiol-terminated disaccharide to immobilize the ligand through addition to the maleimide groups. We used two lectins of different sizes (peanut agglutinin and wheat germ agglutinin) to probe the sensitivity limits of the plasmonic crystals.

SAMDI MS[27,28] was used to quantify the surface coverage ratio of maleimide on the uniformly coated and patterned surfaces. The representative mass spectra collected after disaccharide and protein immobilization on patterned and uniformly coated plasmonic crystals for sensing peanut agglutinin and wheat germ agglutinin are shown in Figures 2

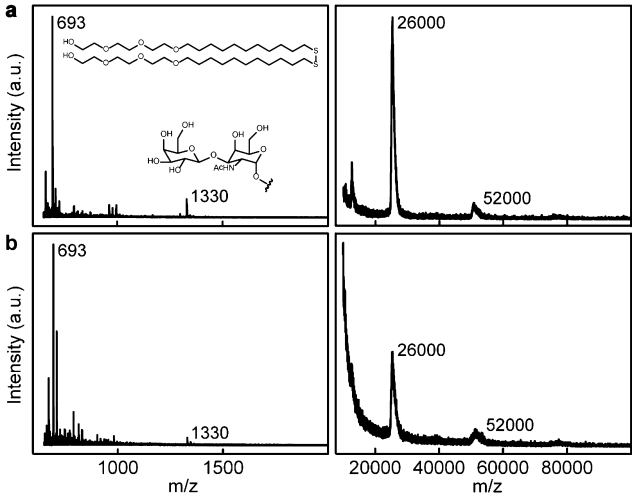

Figure 2. SAMDI characterization of the surface chemistry of Au plasmonic crystal with pyramidal pits used in the real-time measurements of peanut agglutinin (a tetrameric protein, MW = 120 kDa) binding to Galβ(1, 3)GalNAc for (a) uniformly coated and (b) selectively functionalized surfaces. The mass spectra show that the disaccharide reacted completely with the maleimide and the changes in relative surface coverage between the uniformly coated and selectively patterned samples.

and 3, respectively. Taking the ratio of the areas under the mass peaks of the disaccharides with respect to EG3, which acts as an internal standard, allowed us to characterize semiquantitatively the differences in surface coverage between patterned and uniformly coated surfaces. We determined that the patterned substrates displayed the immobilized ligand at 30% of the quantity present on the uniformly coated substrates. These results are consistent with surface area calculations of the plasmonic crystals, where pyramidal pits comprised approximately 30% of the total surface area of the substrate. Furthermore, the intensities of the peaks qualitatively showed that the patterned substrates exhibited a reduced ligand coverage.

We performed real-time measurements of the binding of lectin to the immobilized carbohydrates by tracking the dip position of the strongest resonance of the Au plasmonic crystal, the (−1, 0) SPP mode (Figure 4) at excitation angles θ = 10°−60°. The calculated reflection spectra showed good agreement with the measured spectra, validating the model and enabling simulations of the electromagnetic field distributions.

The normalized (−1, 0) SPP resonances of the plasmonic crystals increased in intensity and decreased in line width as θ increased, which suggest that high θ is optimal for sensing, improving both the signal and resolution of the biosensor.

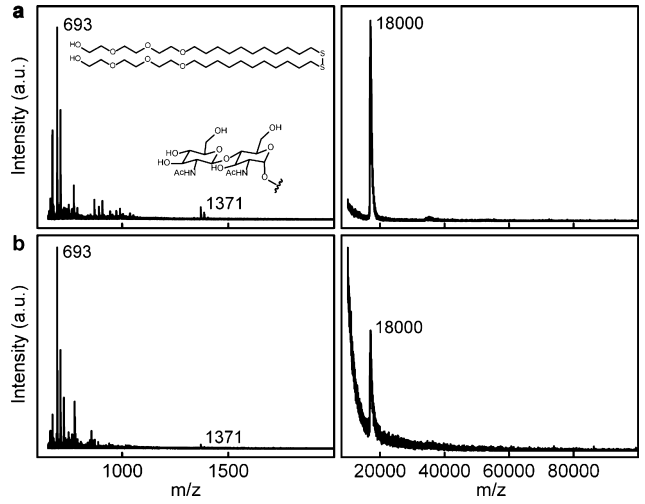

Figure 3. SAMDI characterization of the surface chemistry of Au plasmonic crystals with pyramidal pits used in the real-time measurements of wheat germ agglutinin (a dimeric protein, MW = 36 kDa) binding to GlcNAcβ(1, 4)GlcNAc for (a) uniformly coated and (b) selectively functionalized surfaces.

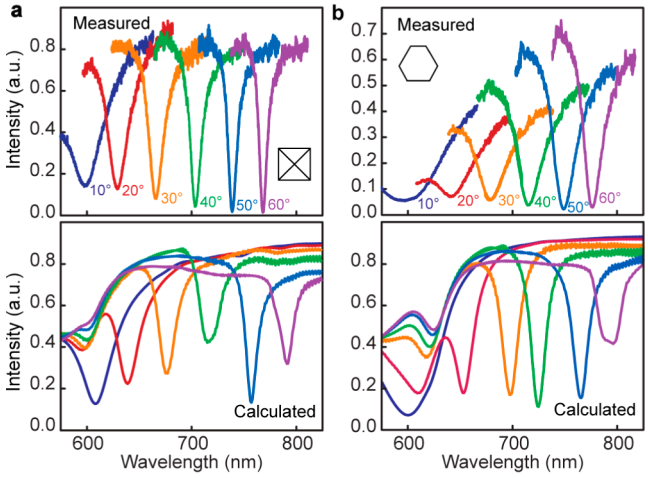

Figure 4. Angle-dependent optical properties are characterized by narrow and high contrast resonances useful for biosensing. Measured and calculated angle-resolved resonances of Au plasmonic crystals with (a) pyramidal and (b) triangular prism-shaped unit cells in a hexagonal array (a_0 = 400 nm). The measured spectra were cropped so that each SPP mode could be seen clearly.

These angle-dependent resonant properties are observed because the propagation length of the SPPs increases as θ increases, which enable them to couple with more unit cells on the plasmonic crystal surface. Notably, the line widths and intensities of the SPP resonances were narrower and higher for pyramidal plasmonic crystals (Figure 4a) compared to triangular prism plasmonic crystals (Figure 4b). Plasmonic crystals with pyramidal pits exhibited high contrast resonances with narrower spectral bandwidths at all θ compared to plasmonic crystals with triangular prism-shaped pits.

Although the optical data suggest that θ = 60° is the best angle for biosensing using our platform, we chose to monitor a dip generated at a lower excitation angle, θ = 30° ($\lambda_{30°}$ = 663 nm), which is the most intense SPP resonance that could be measured in our setup for real-time measurements.[14] The reason for this selection is that the light beam spreads out over

dx.doi.org/10.1021/jp401598a | J. Phys. Chem. C 2013, 117, 5286−5292

a larger area at higher excitation angles, which results in a decrease in intensity. The optical data in Figure 4a were normalized to reflection from a flat Au film.

Sensorgrams were measured to investigate how patterning analyte in the localized fields affected the performance of the plasmonic crystals. The dynamic sensor response (wavelength shift, $\Delta\lambda$) induced by a 5 μM solution of peanut agglutinin injected at a lateral flow rate of 100 μL/min was collected at a 0.5 s time resolution. Saturation binding generated a 2-nm shift on a uniformly coated surface that presented ligand at a density of 5% (Figure 5a, solid line). A 1.3-nm shift was observed for the patterned surface (Figure 5a, dotted line), which is characterized by a total surface ligand density of 1.5%. This surface concentration corresponds to on average 7 proteins bound in each pyramidal unit cell when the peanut agglutinin was approximated as a hard sphere (hydrodynamic radius, R_h = 4 nm) and close packing was assumed. Surprisingly, the patterned substrate generated a response two times greater than expected (~0.6 nm), where the wavelength shift is typically correlated with the quantity of molecules on a surface.[29] This increase in response from selective patterning suggests that local fields supported by the pits contribute to the increased surface sensitivity.

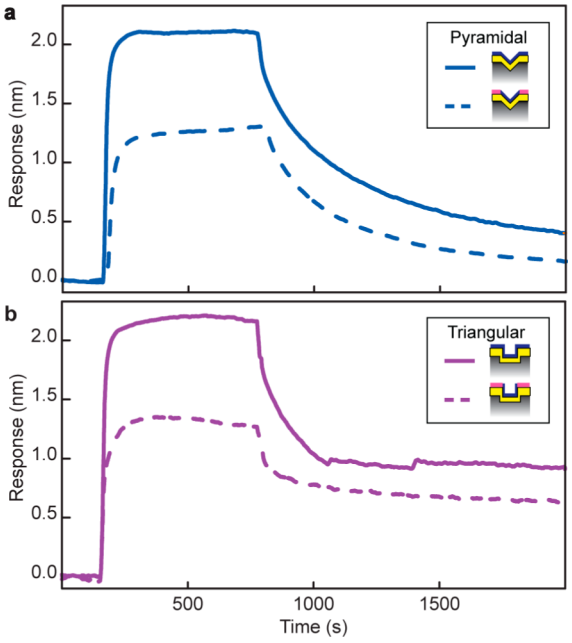

Figure 5. Binding of peanut agglutinin to localized EM regions enhances sensitivity for biosensing. Sensorgrams were generated by monitoring the θ = 30° resonance. An increase in sensitivity resulted from analyte confined in the (a) pyramidal and (b) triangular pits.

Changing the geometry of the 3D unit cell can alter the far-field and near-field optical properties of plasmonic crystals. Nanostructures with well-defined edges and sharp asperities support highly confined localized EM fields.[30] To differentiate between the local field effects and the influence of unit cell shape, we created a plasmonic crystal with triangular prism-shaped pits that had vertical sidewalls that formed a step-edge with the top surface; the total surface area was the same as substrates with pyramidal pits. Binding curves were generated by monitoring the plasmon dip at θ = 30° ($\lambda_{30°}$ = 673 nm) (Figure 4b) for the binding of peanut agglutinin to the triangular prism substrate. The sensing response was $\Delta\lambda$ = 2 nm from a uniformly coated (Figure 5b, solid line) and $\Delta\lambda$ = 1.4 nm from a patterned (Figure 5b, dotted line) triangular prism crystal. These surface sensitivities are similar to those observed for the pyramidal pits.

Finite difference time domain (FDTD) methods were used to visualize the EM field distributions in the pyramidal and triangular prism unit cells. At the resonance condition for different θ, strong fields were localized at the edges where the sidewalls of the pits intersected the flat surface of the substrate for both the pyramidal and triangular prism crystals (Figure 6). The electromagnetic fields with the highest intensities (up to 10^2) occurred at lower θ. In contrast, the SPP intensities are lower (10^0–10^1) than the local enhancements, and the field decay lengths increased at higher θ, as expected for continuous metal films.

Notably, the sharp edges of the triangular prism supported field concentrations of higher intensity (1 order of magnitude) than those sustained on the pyramidal pits. However, the sensing responses were the same for both structures, which can be attributed to similar localized field volumes. This observation could be interpreted as an advantage in terms of sensitivity for the selective surface functionalization of plasmonic crystals because fewer molecules contribute to the signal.

Correlating the FDTD intensity maps with the angle-resolved spectra, we found that the desired far-field optical properties (high intensity and narrow bandwidth at high θ) and near-field characteristics (short decay lengths at low θ) for biosensing are in competition. The broad and less intense SPP resonances of the triangular prism plasmonic crystals may

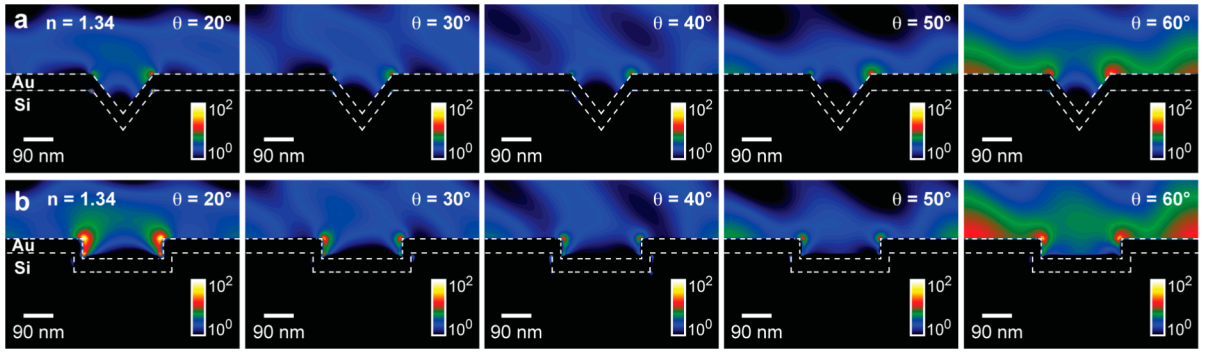

Figure 6. Near-field, $|E|^2$, calculations for plasmonic crystals with (a) pyramidal and (b) triangular unit cells at θ = 20°, 30°, 40°, 50°, and 60° show EM fields localized at the edges of the pits.

dx.doi.org/10.1021/jp401598a | J. Phys. Chem. C 2013, 117, 5286–5292

counteract the benefits of the high-intensity localized EM fields supported by the pits. This result suggests that the effects of the optical near- and far-fields must be balanced to achieve optimal sensor performance and that unit cell geometry may not be the most critical parameter in sensor design.

For new biosensing platforms to be useful, real-time binding responses should be similar to those determined by SPR. To determine how different surface treatments and unit cell shapes affected the kinetics of protein binding, we analyzed the real-time binding of peanut agglutinin to disaccharide Galβ(1, 3)GalNAc on the plasmonic crystals. Figure 7 presents the log

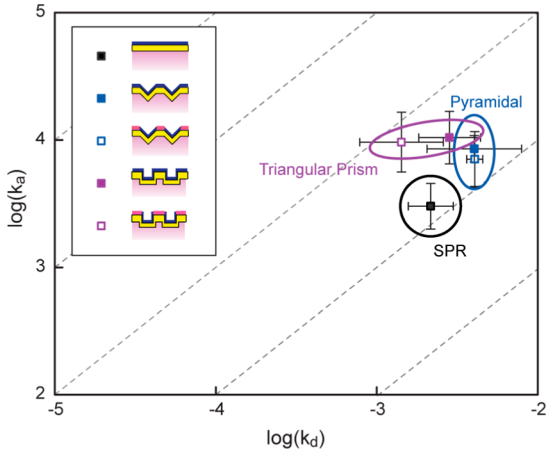

Figure 7. Plasmonic crystals with different unit cell geometries and surface chemistry do not affect protein-binding dynamics compared to SPR. Kinetic constants determined by fitting the sensorgrams generated by conventional SPR (flat Au film) and the Au plasmonic crystals with the Langmuir model. Average rates of association and dissociation of peanut agglutinin to surfaces presenting Gal-β1,3-GalNAc were similar among all substrate types and surface modification schemes (uniformly coated: solid markers; and selectively functionalized: open markers). The error bars represent the standard deviation determined from n = 4–6 data points.

k_a vs log k_d plot for association and dissociation constants from binding curves collected by and from both patterned and uniformly coated substrates with pyramidal and triangular prism pits. The average k_a and k_d values were clustered in the region where the affinity constant is 10^{-4}–10^{-5} M, which is consistent with reported values for peanut agglutinin binding determined by SPR. In addition, the kinetic constants were within one standard deviation of each other and not significantly different. This result indicates that surface topography and molecular patterning do not affect dynamic protein interactions at a Au surface, suggesting that the plasmonic crystals and the selective patterning are viable substrates and surface modification strategies for implementation in future sensor designs. Although each surface generates similar kinetic results, the shape of the triangular prism appears to have a minor effect on how the analyte can be bound within the pits. The vertical sidewalls of the nanostructures could provide pinning points for the buffer transporting the analyte that can physically preclude the buffer from accessing the pits to dissociate the protein. The overall kinetic results, however, verify that surface patterning and unit cell shape will not change the dynamics of protein binding compared to SPR, which allows a range of nanopatterned films to be used as platforms for biosensing.

Angle-resolved real-time measurements were used to distinguish between contributions from nonlocal and localized EM fields to the sensing response. Figure 8a shows that $\Delta\lambda$

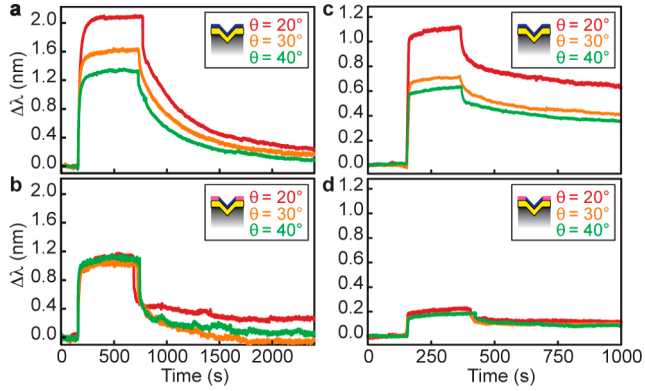

Figure 8. Localized EM fields dominate sensing response at high excitation angles. Sensorgrams measured at θ = 20°, 30°, and 40° of peanut agglutinin bound to (a) uniform and (b) patterned surfaces. Real-time results from binding of wheat germ agglutinin on each substrate are shown in panels c and d, respectively.

decreases when θ increases from 20° to 40° for a pyramidal pit substrate that was uniformly coated. This reduction in surface sensitivity is expected because the SPP decay length increases with resonances that occur at longer wavelengths (higher θ).[14] Notably, the response from selectively functionalized plasmonic crystals was $\Delta\lambda$ = 1 nm (Figure 8b) at all θ, which is consistent with the localized EM fields not changing with θ (Figure 6). The local field enhancements dominate sensitivity more than SPPs as excitation angles increase.

To probe the lower detection limit of the plasmonic crystals, we selected a wheat germ lectin that binds to a disaccharide compatible with the immobilization chemistry used in sample preparation so that the bound proteins are the same fixed distance away from the Au. Sensorgrams collected at a time resolution of 0.1 s as surfaces presenting GlcNAcβ(1, 4)GlcNAc were exposed to a solution of wheat germ agglutinin at higher flow conditions (200 μL/min, 0.625 μM protein) to minimize mass transport-limited effects. The surface sensitivity of uniformly coated substrates decreased from $\Delta\lambda$ = 1.1 to 0.6 nm as θ increased from 20° to 40°. For a selectively functionalized surface, $\Delta\lambda$ = 0.2 nm (28 or fewer proteins per pit) at all θ (Figures 8c,d), which approaches the lower detection capabilities of the system. Differences in molecular size can explain the smaller $\Delta\lambda$ for wheat germ binding compared with peanut agglutinin. At the same surface coverage ratio, proteins with larger areal footprints (100 nm^2 for peanut agglutinin) can form a layer that covers more surface area than those of smaller proteins (25 nm^2 for wheat germ agglutinin), and thus the local environment supports a higher effective n that induces relatively large peak shifts. In addition, analytes of greater size can overlap with more of the localized fields to produce a considerable response.

■ CONCLUSION

In summary, we demonstrated that by patterning receptors in high-EM fields of a nanostructured substrate, the surface sensitivity of plasmonic crystal biosensors could be enhanced. Angle-resolved sensorgrams of peanut agglutinin revealed that the response from localized electric fields dominated at longer

dx.doi.org/10.1021/jp401598a | J. Phys. Chem. C 2013, 117, 5286–5292

wavelengths and higher excitation angles, where the SPP decay lengths increased. Although the optical near field can be tuned for improved sensitivity by designing different unit cell geometries for the plasmonic crystals, these changes can alter the quality of the far-field resonances, which can hinder the local field effects. Hence, careful consideration of the far-field and near-field optical properties, which is dictated by excitation angle, is crucial for optimal performance. Finally, we found that the system is currently limited to detecting proteins >36 kDa but could be improved by adjusting the surface modification chemistry. Overall, localized EM fields play a critical role in boosting the sensitivity of SPP-based sensing platforms. We anticipate that these substrates could be further applied to studying the fundamental interactions of biological molecules on surfaces (e.g., the cell membrane).

AUTHOR INFORMATION

Corresponding Author

*E-mail: todom@northwestern.edu.

Notes

The authors declare no competing financial interest.

ACKNOWLEDGMENTS

This work was supported by the NSF under award no. CHE-105801 (J.L.). A.S. acknowledges the CCNE (5U4CA151880-02) and DARPA (N66001-11-1-4179). M.H. thanks the DoD through the NDSEG. This work made use of the NUANCE Center facilities, which are supported by the NSF-MRSEC, NSF-NSC, the Keck Foundation, and the Materials Processing and Microfabrication Facility, which is supported by the MRSEC program of the NSF (DMR-1121262).

REFERENCES

(1) Arlett, J. L.; Myers, E. B.; Roukes, M. L. Comparative Advantages of Mechanical Biosensors. *Nat. Nanotechnol.* **2011**, *6*, 203−215.

(2) Willets, K. A.; Van Duyne, R. P. Localized Surface Plasmon Resonance Spectroscopy and Sensing. *Annu. Rev. Phys. Chem.* **2007**, *58*, 267−297.

(3) Lee, S.; Mayer, K. M.; Hafner, J. H. Improved Localized Surface Plasmon Resonance Immunoassay with Gold Bipyramid Substrates. *Anal. Chem.* **2009**, *81*, 4450−4455.

(4) Mayer, K. M.; Hao, F.; Lee, S.; Nordlander, P.; Hafner, J. H. A Single Molecule Immunoassay by Localized Surface Plasmon Resonance. *Nanotechnology* **2010**, *21*, 255503.

(5) Mayer, K. M.; Lee, S.; Liao, H.; Rostro, B. C.; Fuentes, A.; Scully, P. T.; Nehl, C. L.; Hafner, J. H. A Label-Free Immunoassay Based Upon Localized Surface Plasmon Resonance of Gold Nanorods. *ACS Nano* **2008**, *2*, 687−692.

(6) Nusz, G. J.; Marinakos, S. M.; Curry, A. C.; Dahlin, A.; Hook, F.; Wax, A.; Chilkoti, A. Label-Free Plasmonic Detection of Biomolecular Binding by a Single Gold Nanorod. *Anal. Chem.* **2008**, *80*, 984−989.

(7) Zijlstra, P.; Paulo, P. M. R.; Orrit, M. Optical Detection of Single Non-Absorbing Molecules Using the Surface Plasmon Resonance of a Gold Nanorod. *Nat. Nanotechnol.* **2012**, *7*, 379−382.

(8) Ament, I.; Prasad, J.; Henkel, A.; Schmachtel, S.; Sönnichsen, C. Single Unlabeled Protein Detection on Individual Plasmonic Nanoparticles. *Nano Lett.* **2012**, *12*, 1092−1095.

(9) Jonsson, M. P.; Dahlin, A. B.; Feuz, L.; Petronis, S.; Höök, F. Locally Functionalized Short-Range Ordered Nanoplasmonic Pores for Bioanalytical Sensing. *Anal. Chem.* **2010**, *82*, 2087−2094.

(10) Feuz, L.; Jönsson, P.; Jonsson, M. P.; Höök, F. Improving the Limit of Detection of Nanoscale Sensors by Directed Binding to High-Sensitivity Areas. *ACS Nano* **2010**, *4*, 2167−2177.

(11) Ferreira, J.; Santos, M. J. L.; Rahman, M. M.; Brolo, A. G.; Gordon, R.; Sinton, D.; Girotto, E. M. Attomolar Protein Detection Using In-Hole Surface Plasmon Resonance. *J. Am. Chem. Soc.* **2008**, *131*, 436−437.

(12) Wei, R.; Gatterdam, V.; Wieneke, R.; Tampe, R.; Rant, U. Stochastic Sensing of Proteins With Receptor-Modified Solid-State Nanopores. *Nat. Nanotechnol.* **2012**, *7*, 257−263.

(13) Feuz, L.; Jonsson, M. P.; Höök, F. Material-Selective Surface Chemistry for Nanoplasmonic Sensors: Optimizing Sensitivity and Controlling Binding to Local Hot Spots. *Nano Lett.* **2012**, *12*, 873−879.

(14) Gao, H.; Yang, J.-C.; Lin, J. Y.; Stuparu, A. D.; Lee, M. H.; Mrksich, M.; Odom, T. W. Using the Angle-Dependent Resonances of Molded Plasmonic Crystals to Improve the Sensitivities of Biosensors. *Nano Lett.* **2010**, *10*, 2549−2554.

(15) Stewart, M. E.; Mack, N. H.; Malyarchuk, V.; Soares, J. A. N. T.; Lee, T.-W.; Gray, S. K.; Nuzzo, R. G.; Rogers, J. A. Quantitative Multispectral Biosensing and 1D Imaging Using Quasi-3D Plasmonic Crystals. *P. Natl. Acad. Sci.* **2006**, *103*, 17143−17148.

(16) Gao, H.; Henzie, J.; Lee, M. H.; Odom, T. W. Screening Plasmonic Materials Using Pyramidal Gratings. *Proc. Natl. Acad. Sci.* **2008**, *105*, 20146−20151.

(17) Yang, J.-C.; Gao, H.; Suh, J. Y.; Zhou, W.; Lee, M. H.; Odom, T. W. Enhanced Optical Transmission Mediated by Localized Plasmons in Anisotropic, Three-Dimensional Nanohole Arrays. *Nano Lett.* **2010**, *10*, 3173−3178.

(18) Houseman, B. T.; Gawalt, E. S.; Mrksich, M. Maleimide-Functionalized Self-Assembled Monolayers for the Preparation of Peptide and Carbohydrate Biochips. *Langmuir* **2002**, *19*, 1522−1531.

(19) Houseman, B. T.; Mrksich, M. The Role of Ligand Density in the Enzymatic Glycosylation of Carbohydrates Presented on Self-Assembled Monolayers of Alkanethiolates on Gold. *Angew. Chem., Int. Ed.* **1999**, *38*, 782−785.

(20) Milton, J. D.; Fernig, D. G.; Rhodes, J. M. Use of a Biosensor to Determine the Binding Kinetics of Five Lectins for Galactosyl-*N*-Acetylgalactosamine. *Glycoconjugate J.* **2001**, *18*, 565−569.

(21) Henzie, J.; Kwak, E.-S.; Odom, T. W. Mesoscale Metallic Pyramids With Nanoscale Tips. *Nano Lett.* **2005**, *5*, 1199−1202.

(22) Henzie, J.; Lee, M. H.; Odom, T. W. Multiscale Patterning of Plasmonic Metamaterials. *Nat. Nanotechnol.* **2007**, *2*, 549−554.

(23) Ban, L.; Pettit, N.; Li, L.; Stuparu, A. D.; Cai, L.; Chen, W.; Guan, W.; Han, W.; Wang, P. G.; Mrksich, M. Discovery of Glycosyltransferases Using Carbohydrate Arrays and Mass Spectrometry. *Nat. Chem. Biol.* **2012**, *8*, 769−773.

(24) Baek, M.-G.; Roy, R. Simultaneous Binding of Mouse Monoclonal Mntibody and Streptavidin to Heterobifunctional Dendritic L-lysine Bore Bearing T-antigen Tumor Marker and Biotin. *Biorg. Med. Chem.* **2001**, *9*, 3005−3011.

(25) Palik, E. D. Handbook of Optical-Constants. *J. Opt. Soc. Am. A* **1984**, *1*, 1297−1297.

(26) Johnson, P. B.; Christy, R. W. Optical Constants of the Noble Metals. *Phys. Rev. B* **1972**, *6*, 4370−4379.

(27) Mrksich, M. Mass Spectrometry of Self-Assembled Monolayers: A New Tool for Molecular Surface Science. *ACS Nano* **2008**, *2*, 7−18.

(28) Su, J.; Mrksich, M. Using Mass Spectrometry to Characterize Self-Assembled Monolayers Presenting Peptides, Proteins, and Carbohydrates. *Angew. Chem., Int. Ed.* **2002**, *41*, 4715−4718.

(29) Schasfoort, R. B. M.; Tudos, A. J. *Handbook of Surface Plasmon Resonance*; The Royal Society of Chemistry: Cambridge, UK, 2008.

(30) Mayer, K. M.; Hafner, J. H. Localized Surface Plasmon Resonance Sensors. *Chem. Rev.* **2011**, *111*, 3828−3857.